Article

Virtual Synchronous Generator Control of Grid Connected Modular Multilevel Converters with an Improved Capacitor Voltage Balancing Method

Haroun Bensiali [1], Farid Khoucha [1], Abdeldjabar Benrabah [1], Lakhdar Benhamimid [1] and Mohamed Benbouzid [2,*]

1 Ecole Militaire Polytechnique, UER ELT, Algiers 16111, Algeria; harounbensiali@gmail.com (H.B.); farid.khoucha@emp.mdn.dz (F.K.); abdeldjabar.benrabah@emp.mdn.dz (A.B.); benhamimidlakhdareeei@gmail.com (L.B.)
2 Institut de Recherche Dupuy de Lôme (UMR CNRS 6027), University of Brest, 29238 Brest, France
* Correspondence: mohamed.benbouzid@univ-brest.fr

Abstract: Modular multilevel converters have emerged as a common solution in high-voltage and medium-voltage applications due to their scalability and modularity. However, these advantages come at the cost of increased control complexity, particularly when compared to other multilevel converter topologies. This paper proposes a new combined control strategy based on virtual synchronous generator (VSG) control and capacitor voltage balancing (CVB) method. The VSG control is applied for power sharing and inertia emulation to increase the dynamic response and improve system stability while the CVB method is used to redistribute the energy stored in the capacitors of the submodules (SMs) in order to ensure uniform voltage levels and equalize the voltage across the capacitors. The simulation results as well as experimental ones confirm the feasibility and effectiveness of the proposed method, enhancing the performance of the energy conversion system.

Keywords: capacitor voltage balancing; modular multilevel converter; grid-connected MMC; virtual synchronous generator

1. Introduction

The field of integrating renewable energy sources into the electricity grid presents both significant challenges and opportunities. The challenges include the need to ensure the efficient integration of renewable energy while maintaining the stability and reliability of the electricity grid [1,2]. Fluctuations in renewable energy generation can lead to rapid variations in the power injected into the grid, requiring advanced control strategies to ensure effective regulation [3].

Modular multilevel converters (MMCs) play a key role in the integration of renewable energies, offering an optimal solution for connecting these resources to the power grid [4–6]. Their modular and scalable structure enables energy to be converted efficiently while improving grid stability [7,8]. The present study focuses on medium-voltage applications in a grid-connected system, where the MMC serves as a critical interface connecting renewable energy sources to the power grid, facilitating efficient energy transfer and integration, using an additional converter (chopper or rectifier). In this configuration, renewable energy sources are linked to the DC side, efficient energy conversion to AC for seamless and stable grid integration. This approach tackles the challenges of variability in renewable energy output while maintaining system stability and reliability. Notably,

due to their excellent scalability, MMCs can also be specifically adapted and optimized to meet the demands of high-voltage applications, such as high-voltage direct current (HVDC) transmission systems [9,10]. However, this integration comes with challenges, such as the need to achieve optimum performance in terms of power regulation, reducing unwanted circulating currents, minimizing disturbances on the DC side, and balancing the voltages of the SM capacitors. Studies highlight the importance of MMC energy control in system dynamics during grid formation and tracking operations [11]. Furthermore, the complexity of MMC topologies and the demand for efficient control strategies present additional obstacles [5,12]. These challenges require innovative control approaches capable of addressing the complexities of MMCs while optimizing their dynamic behavior.

The proposed combined control strategy, based on Virtual Synchronous Generator (VSG) control and Capacitor Voltage Balancing (CVB), aims to overcome these shortcomings by improving stability and performance [13,14]. This innovative approach attempts to overcome the limitations and complexities identified in existing MMC control methods [15].

The VSG control focuses on power management and inertia imitation, which helps to improve the dynamic response and overall stability of the system [16,17]. By successfully managing power sharing, VSG enhances the MMC's ability to respond dynamically to power variations, ensuring optimal operation under a range of conditions [18,19].

The CVB method is a crucial element in maintaining uniform voltage levels and equalizing voltages between capacitors within the SM in MMC. Notable for its sensorless operation, the CVB uses estimation techniques, based on mathematical models, to derive capacitor voltages [20]. This sensorless approach improves control efficiency by reducing reliance on physical sensors, simplifying hardware complexity and potentially reducing overall system costs.

In addition, the CVB method aims to strategically minimize the number of switching events in the MMC, optimizing switching schemes to balance capacitor voltages with a minimum number of events [21,22]. This reduction in switching events not only enhances system reliability but also contributes to a reduction in switching losses, leading to an overall improvement in energy efficiency [23]. To calculate the switching losses of the converter, it is essential to obtain the energy losses at each turn-on and turn-off stage of the insulated gate bipolar transistors (IGBTs) and freewheeling diodes (FWDs). Consequently, reducing switching events has a direct impact on reducing switching losses [23].

The novelty of this paper lies in the proposed combined control strategy that integrates VSG control with a simplified CVB method for grid-connected MMC systems. The paper presents a comprehensive analysis of the effectiveness of the proposed control strategy, comparing it with conventional approaches of decoupled PQ control, VSG control, and combined CVB-PQ control. The results highlight the suitability of CVB-VSG for the control of MMC-based grid-connected systems, highlighting its potential benefits in minimizing circulating currents, reducing DC-side disturbances, balancing capacitor voltages, eliminating the need for extensive sensor deployment, and reducing computational requirements.

The rest of the paper is organized as follows: Section 2 presents the modeling of the MMC and its operating principle. The proposed control is presented in Section 3. The simulation and experimental results are discussed in Section 4. Finally, conclusions are drawn in the Section 5.

2. MMC Modeling and Operating Principle

Figure 1a shows the schematic diagram of the MMC. It consists of three identical phases connected in parallel and powered by a DC voltage source. Each phase consists of an upper and a lower arm, each arm combines N SMs in series with an inductor L_{arm}.
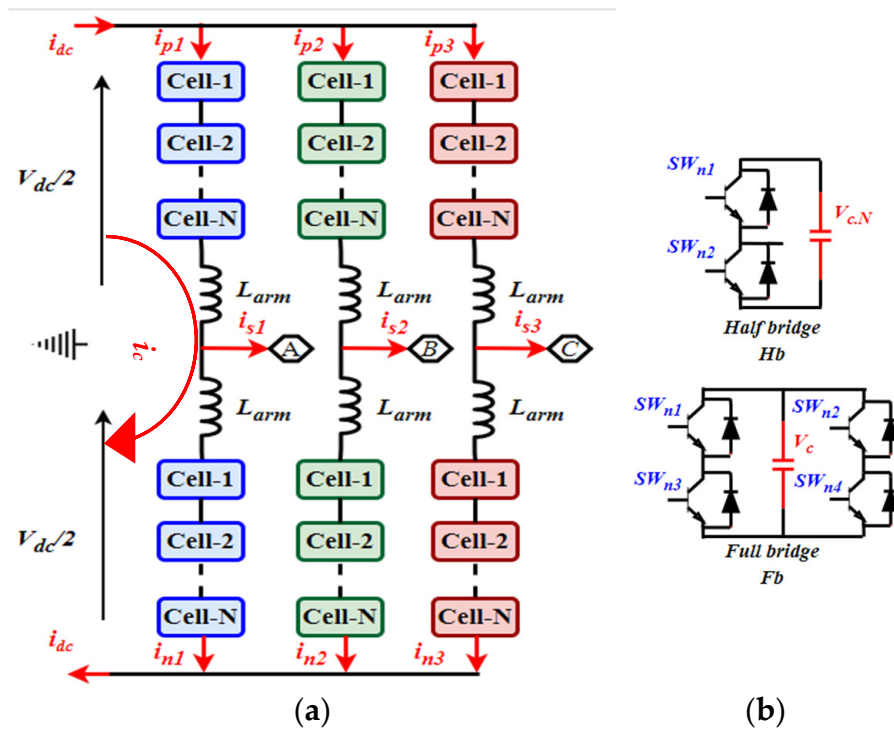
Figure 1. Multilevel converter topology: (**a**) MMC; (**b**) half-bridge and full-bridge SM.

The most commonly used SMs are half-bridge SM and full-bridge SM [24,25]. The half-bridge SM uses two IGBT switches with two antiparallel diodes and a DC storage capacitor, and the full-bridge SM uses four IGBT switches with four antiparallel diodes and a capacitor. The half-bridge SM quickly became the dominant choice of converter topology. This topology offers low switching losses, cost-effectiveness, and minimal AC distortion, all of which contribute to better energy efficiency. This is what motivated the choice of the half-bridge MMC in our work. The existing SMs in the arm are controlled so that the capacitor is inserted into the circuit or bypassed. The schematic diagrams of the half-bridge SM and full-bridge SM are shown in Figure 1b.

The basic control principle of MMCs is analyzed based on the dynamics of each converter phase. Applying Kirchhoff's voltage law on an arbitrary phase of Figure 1a gives:

$$i_p = \frac{i_s}{2} + \frac{i_{dc}}{3} + i_c \tag{1}$$

$$i_n = -\frac{i_s}{2} + \frac{i_{dc}}{3} + i_c \tag{2}$$

$$-\frac{v_{dc}}{2} + v_p + R i_p + L_{arm}\frac{di_p}{dt} + L_T\frac{di_s}{dt} + v_g = 0 \tag{3}$$

$$\frac{v_{dc}}{2} - v_n - R i_n - L_{arm}\frac{di_n}{dt} + L_T\frac{di_s}{dt} + v_g = 0 \tag{4}$$

where R and L_T are the equivalent resistance in the loop and transformer leakage reactance, respectively. i_p and i_n are the upper and lower arm current, i_s is the phase current, i_{dc} is the current of the continuous bus, i_c is the circulation current, v_{dc} is the bus voltage, v_p and v_n are the upper and lower arm voltage, and v_g is the grid voltage.

In an MMC, i_c refers to the unwanted current that flows within the MMC's phase legs, between the upper and lower arms, without contributing to the output power delivered to the load or grid. It arises mainly due to voltage differences between the SM capacitors in the arms and the DC-link voltage. These differences occur naturally because of the switching

actions and the charging/discharging of capacitors as the MMC generates the desired AC output waveform.

Adding (3) and (4) can obtain a dynamic equation for the output current:

$$L_{eq}\frac{di_s}{dt} = v_s - \frac{R}{2}i_s - v_g \tag{5}$$

where:

$$\begin{aligned} v_s &= \frac{v_n - v_p}{2} \\ i_s &= i_p - i_n \\ L_{eq} &= \frac{L_{arm}}{2} + L_T \end{aligned}$$

with v_s is the inner EMF, which drives the converter phase current i_s, and L_{eq} is the equivalent reactance in the loop. From (5) we obtain:

$$\frac{di_s}{dt} = \frac{1}{L_{eq}}v_s - \frac{R}{2L_{eq}}i_s - \frac{1}{L_{eq}}v_g \tag{6}$$

3. The Proposed Control System

In order to improve the control performance of the MMC system, a novel control strategy is introduced that combines the VSG control with the capacitor voltage balancing CVB method. The VSG control is utilized to enhance dynamic response, improve system stability, and facilitate power sharing and inertia emulation while the CVB method is employed to redistribute the energy stored in the SMs capacitors, ensuring uniform voltage levels and equalizing the voltage across the capacitors. The proposed control design for the grid-connected MMC is shown in Figure 2.
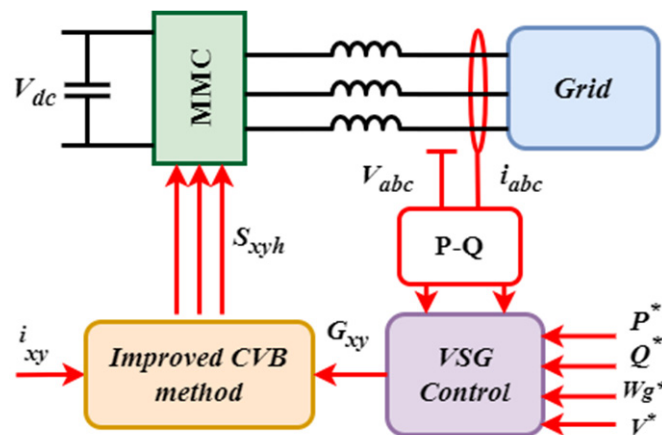

Figure 2. Block diagram of the proposed CVB-VSG control.

3.1. VSG-Based Control of Grid-Connected MMC

The VSG-based control is applied to emulate the behavior of a synchronous generator in the grid-connected MMC system. It enables the MMC to provide inertial response and frequency regulation similar to conventional synchronous generators. The VSG control scheme is illustrated in Figure 3.

The aim of this control is to provide active and reactive power control, voltage regulation, and frequency support similar to a synchronous generator. The VSG control introduces frequency and voltage droop characteristics, which are typical features of synchronous generators. By utilizing droop control, the MMC adjusts its output power based on changes in grid frequency and voltage. This behavior provides inertia and stability support to the grid [17,25].
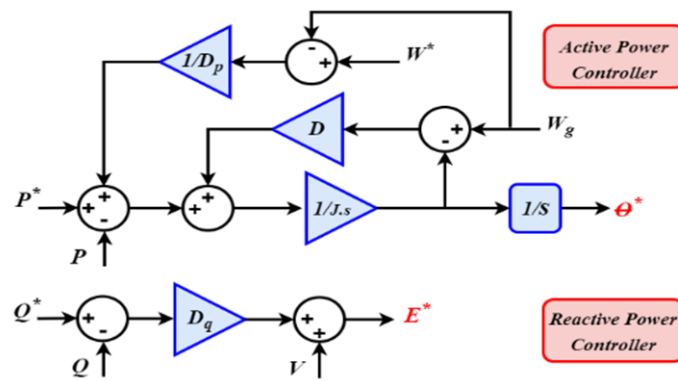
Figure 3. VSG based control scheme.

The mathematical model of the VSG is obtained from the second-order model of a synchronous generator, the mechanical rotation equation of the rotor, and the voltage equation of the stator [25–27].

$$J\frac{d\omega}{dt} = \frac{P_m - P_e}{\omega} - D(\omega - \omega_g) \tag{7}$$

$$e_{abc} = v_{abc} - Ri_{abc} - L\frac{di_{abc}}{dt} \tag{8}$$

where P_m is the mechanical power; P_e is the electromagnetic power; J and D represent the inertia and damping, respectively; w is the rotor angular frequency; w_g is the actual angular frequency of the grid; and e_{abc}, v_{abc}, and i_{abc} are the excitation voltage, terminal voltage, and stator current of the SG, respectively. R is the armature resistance and L is the synchronous reactance.

The VSG droop control mathematical model for controlling frequency and voltage is expressed as follows:

$$\omega_g = \omega_N + D_P(P_N - P) \tag{9}$$

$$U = U_N + D_q(Q_N - Q) \tag{10}$$

where P_N and Q_N are the rated active power and reactive power, respectively; P and Q are the VSG active and reactive powers, respectively; D_P is the P-ω droop coefficient; D_q is the Q-U droop coefficient; U_N is the rated voltage amplitude; and ω_N is the rated angular frequency.

The VSG control is designed to emulate the behavior of a synchronous generator. It relies on equations such as mechanical rotation (Equation (7)) and droop control (Equations (9) and (10)) to determine the active and reactive power (P, Q). These measured values, along with the reference values P^* and Q^*, are used to adjust the outputs θ^* (the phase angle reference) and E^* (the voltage amplitude reference). The PWM modulator then uses these outputs. The VSG control strategy allows for the emulation of key dynamic characteristics typically exhibited by traditional synchronous generators, specifically their inertial response and ability to regulate frequency, it ensures that the MMC can contribute to stabilizing the grid, especially under conditions where renewable energy sources introduce variability or disturbances.

In our VSG control scheme (illustrated in Figure 3), the measured active and reactive power (P and Q) are compared to their respective reference values (P^* and Q^*), which are defined based on the desired operating conditions or the nominal values of the system. The differences between these measured and reference values are used in droop control equations to generate frequency and voltage deviations, resulting in the outputs θ^* and E^*. These outputs are then fed to the PWM modulator: θ^* adjusts the synchronization and

phase of the switching signals (thus controlling the active power by synchronizing the converter with the grid frequency), while E^* defines the amplitude of the synthesized AC voltage (thus regulating the reactive power).

The VSG control employs a droop-based control strategy, where grid frequency variations (linked to active power) influence the phase angle, thereby adjusting the output power. Conversely, the reactive power Q is controlled through the voltage magnitude E^*. The VSG adjusts the output voltage according to the reactive power demand, ensuring that the system remains stable and responsive to changes in grid conditions.

3.2. Improved CVB Method

The capacitor voltage imbalance not only compromises the converter efficiency but can also lead to reduced system reliability and increased maintenance costs [28]. Therefore, the development of effective control strategies to mitigate and manage capacitor voltage imbalances is a key issue in the design and operation of MMCs [29].

Several research efforts have been conducted to address this challenge, focusing on various control strategies [30]. Previous works have explored traditional proportional-integral (PI) controllers [31] and model predictive control [32–34]. Nevertheless, these methods often depend on precise sensor feedback, which increases both the complexity and the cost of the overall system, necessitating additional hardware and sophisticated signal processing to ensure reliable performance [35].

To optimize capacitor voltage balancing algorithms, some researchers have proposed several solutions, including reducing the computational load on the processor or a new MMC topology that has the ability to self-balance the capacitor voltage. By using auxiliary circuits and not requiring information about the voltage of each SM capacitor, voltage sensor and processor computational loads are reduced. Reference [36] proposed a new MMC topology with capacitor voltage self-balancing capabilities, relying on three voltage sensors and eliminating the need for sorting algorithms. However, while this method reduces control complexity, it needs auxiliary circuits and three voltage sensors. Reference [37] proposed a new method for estimating the SM capacitor voltage using one voltage sensor per arm and one current sensor at the converter output. The method is based on a Kirchhoff voltage law and circuit relations governing the AAMC; however, it needs six voltage sensors and three current sensors to realize the voltage balancing. A sensorless capacitor voltage balancing technique was proposed in [38]; it uses a logical permutation sequence for capacitor voltage balancing in a five-phase MMC. Nevertheless, this strategy does not target a simple three-phase MMC configuration with less control complexity. Using a reduced number of voltage sensors and an estimation technique, reference [39] proposed an approach for monitoring the condition of SM capacitors in MMCs. Nonetheless, one voltage sensor is required for each set of SMs in each arm. Reference [40] proposed a method for estimating the voltages of SM capacitors in an MMC using a Kalman filter with one voltage sensor per arm. The computational complexity of this method is relatively high, requiring significant processing power and real-time resources, which can increase the overall cost and latency of the control system. A technique for balancing capacitor voltages was proposed in [41], using an algorithm for sorting the measured capacitor voltages and selecting the SMs to insert according to the current direction. However, a voltage sensor is required for each SM in each arm.

The above methods reduce the number of sensors to varying degrees, but our proposed CVB method is unique in that it eliminates the need for external sensors, relying on estimation techniques based on mathematical models to predict capacitor voltages [20]. This approach not only simplifies the system architecture by eliminating the need for

additional physical components but also enhances cost efficiency and reduces potential points of failure, relying solely on the robustness of algorithmic computations.

By eliminating the influence of measurement noise, this technique offers significantly better accuracy than the above methods, as well as improved responsiveness to rapid load variations. This is because it optimizes the insertion of SMs via dynamic current-based classification, which limits unnecessary switching and reduces the associated losses.

Thanks to its high adaptability, which allows model parameters to be modified without hardware intervention, this approach not only improves efficiency and simplifies control but also reduces system costs while guaranteeing robust performance under a range of operating conditions. It is therefore a promising solution for improving the reliability and efficiency of MMCs.

This control method relies on controlling the charging and discharging of the SM capacitors based on the direction of the arm current and the instantaneous capacitor voltage using a logic function-based algorithm [21,22,27], as shown in Figure 4.
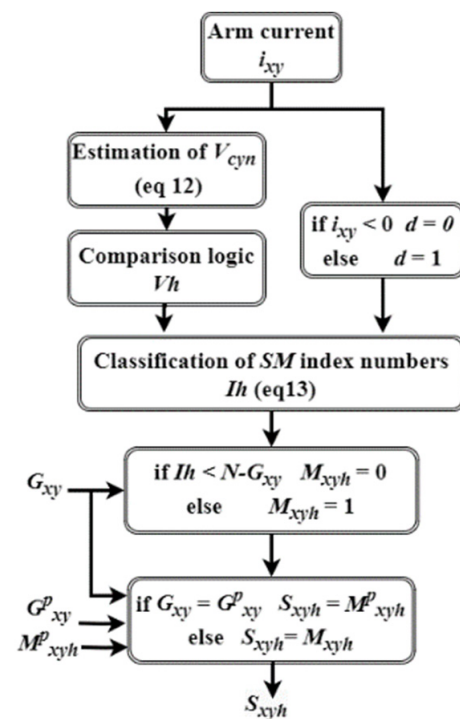

Figure 4. Flowchart of the CVB algorithm.

The proposed CVB method offers several advantages, such as scalability and straightforward programming. It eliminates the need for a *PI* controller to set capacitor voltages and instead utilizes an algorithm based on simple logic comparisons.

In order to implement this CBV method, the capacitor voltages of the SMs in each arm are estimated using the dynamic equation of the SM capacitor voltage:

$$i_{cxyn} = C\frac{dV_{cyn}}{dt} \tag{11}$$

where i_{cxyn} and V_{cyn} represent the SM current and SM capacitor voltage, respectively, with x representing the phase (x = a, b, c) and y representing the arm (y = p, n).

Using *Euler* approximation and assuming a sampling period of T_s, the predicted SM capacitor voltages at discrete time are derived from (12):

$$V_{cyn}(t + T_s) = V_{cyn}(t) + i_{xy}\frac{T_s}{C} \tag{12}$$

where i_{xy} is the upper or lower arm current.

The estimated SM capacitor voltages are introduced into the comparison logic, which compares each capacitor voltage to obtain an index number *Ih*. The highest index number corresponds to the lowest capacitor voltage and vice versa. The arm current direction d is then determined.

The SMs are then sorted in ascending or descending order of SM index numbers according to the direction of the arm current using (13), which presents the actual index number *Ah*:

$$Ah = Ih \times d + (N - 1 - Ih) \times (1 - d) \tag{13}$$

The SMs with the lowest capacitor voltage are inserted for the positive current direction and are charged. Similarly, the SMs with the highest capacitor voltage are inserted for the negative current direction and are discharged.

The required number of inserted SMs G_{xy} is obtained from the output vector generation command VSG. The insertion and bypass (short-circuit) states Mxyh for each SM are generated by comparing the actual index number Ah with the reference index number (N- G_{xy}).

Finally, the calculation optimization is performed by comparing the inserted SMs G_{xy} current number with the inserted SMs G^p_{xy} previous number. If the voltage levels are different, the algorithm applies the new control signals (i.e., $S_{xyh} = M_{xyh}$). Otherwise, the algorithm maintains the previous switching state (i.e., $S_{xyh} = M^p_{xyh}$).

4. Discussion

4.1. Simulation Results

First, numerical simulations are conducted in MATLAB/Simulink (R2021b) environment in order to evaluate the effectiveness of the proposed VSG-based control with the improved CVB method. The obtained results are also compared to the conventional PQ decoupled control with the CVB method. All simulations are performed using the parameters listed in Table 1.

Table 1. Electrical power system parameters.

Parameters	Simulation	Experimental
DC voltage (VDC)	400 V	100 V
AC voltage (VAC)	155 V	30 V
AC frequency	50 Hz	50 Hz
Power active	6–7.5–9 Kw	100–120 W
Number of SMs per arm	2	2
Capacitor value for a SM	50 mF	3.3 mF
Arm inductance/arm resistor	1 mH/0.5 Ω	10 mH/0.5 Ω
Phase inductor/phase resistor	20 mH/0.5 Ω	20 mH/0.5 Ω

Figure 5 presents the simulation results of two control strategies applied to the MMC, namely CVB-PQ control and CVB-VSG control.

The waveforms of current and voltage in the steady-state operation of the MMC and the grid are shown in Figures 5a and 5b, respectively. The estimated capacitor voltages of phase A SMs are illustrated in Figures 5c and 5d for CVB-PQ control and CVB-VSG control, respectively.

When there is a change in injected power to the grid, the capacitor voltages of the SMs deviate to adjust to an equilibrium state, as demonstrated by Figure 5e. The voltage fluctuations of SMs in the same arm are identical and complementary between the upper

and lower arms. The voltage fluctuation range of the SMs is 198.2 V to 198.35 V for
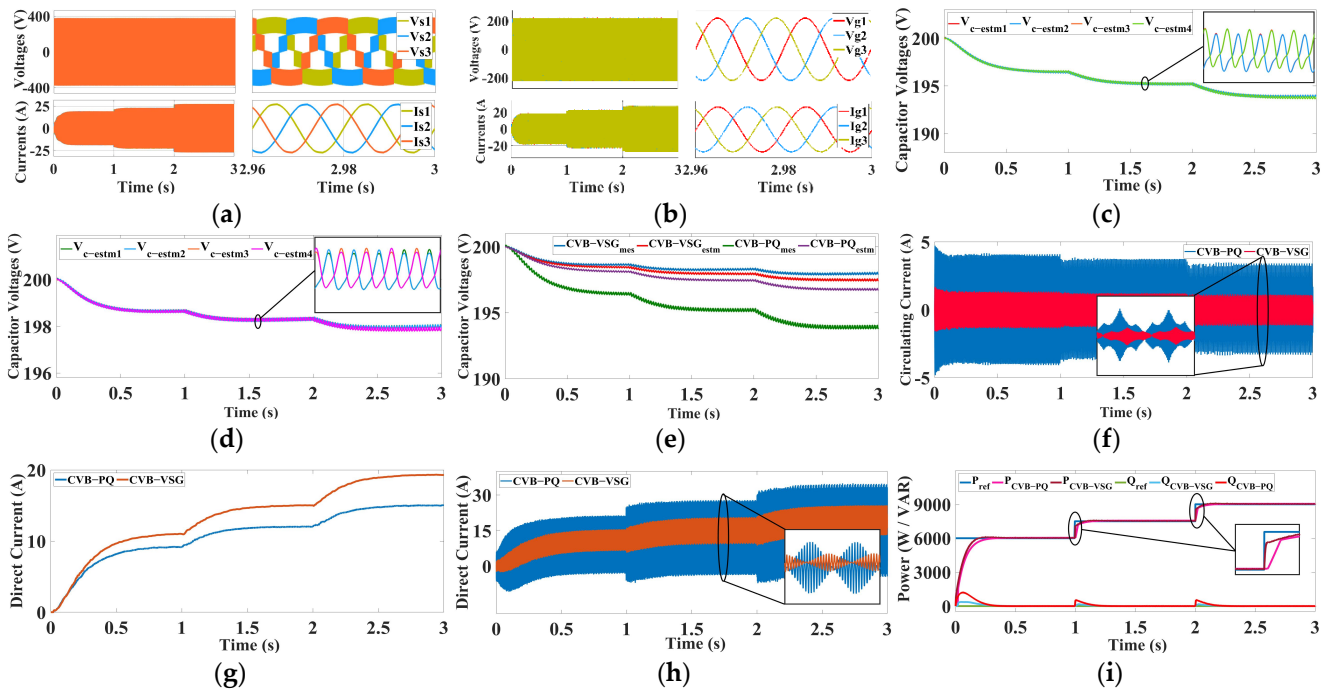CVB-VSG control and 195 V to 195.4 V for CVB-PQ control.

Figure 5. Simulation results of applying CVB−VSG control and CVB−PQ control to the MMC.
(**a**) Three−phase voltages and currents of the MMC. (**b**) Three−phase voltages and currents of
the grid. (**c**) Estimation of the voltages of the SM capacitor of phase A by the CVB−PQ control.
(**d**) Estimation of the voltages of the SM capacitor of phase A by the CVB-VSG control. (**e**) Estimation
and measurement of phase A SM capacitor voltages for both commands. (**f**) Phase A circulating
current. (**g**) Average value of DC current. (**h**) DC current. (**i**) Active and reactive power.

The circulating currents of both CVB-PQ control and CVB-VSG control are presented
in Figure 5f.

The fluctuation of the circulating current is −3.4 A to 3.4 A for CVB-PQ control and
−1.2 A to 1.1 A for CVB-VSG control. Furthermore, as shown in Figure 5g,h, the DC current
is more stable in the case of CVB-VSG control compared to CVB-PQ control. It is observed
that the fluctuations in the DC current for CVB-VSG control are smaller (10 A to 20 A)
compared to CVB-PQ control (from −2 A to 26 A).

Figure 5i clearly demonstrates that the active and reactive powers follow the power
references. However, an important observation is that the response time of CVB-VSG
control is significantly shorter than that of CVB-PQ control during a power reference change.

Regarding the total harmonic distortion (THD) of the alternating currents, it is low in
the case of CVB-VSG control compared to CVB-PQ control, as highlighted in Figure 6.

Table 2 presents the results in numerical form of the relevant measures and indicators
used to evaluate the performance of the CVB-VSG and CVB-PQ control methods. This
enables a precise analysis and a better understanding of the performance of the two
control methods. It becomes easier to identify the advantages and disadvantages of each
control method.

Table 2. Performance evaluation results of CVB-PQ and CVB-VSG.

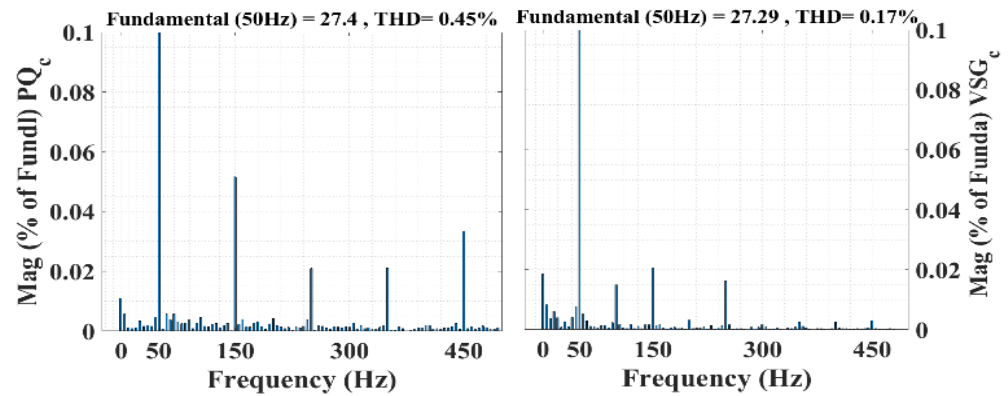| Control	THD	ΔIdc	ΔIcirc	ΔVc	Vcref–Vcestm
CVB-PQ	0.45%	28 A	6.8 A	0.4 V	4.8 V
CVB-VSG	0.17%	10 A	2.3 A	0.15 V	1.7 V

Figure 6. Total harmonic distortion of grid current.

The simulation study aims to investigate the significance of the proposed CVB method and its impact on the performance of the MMC. The study presents the operation of the MMC with the CVB method, depicted in Figure 3, while the operation without the CVB method is illustrated in [19].

The proposed CVB method ensures that the SM capacitor voltages remain at their nominal values. In contrast, in [23], the MMC is controlled using VSG and PQ controls without the CVB. Under this control mode, the SM capacitor voltages deviate from their nominal values, either increasing or decreasing depending on their respective duty cycles.

The CVB method enhances the output voltage waveform of the MMC, reducing the THD and constraining the fluctuations in the SM capacitor voltages and DC current. Consequently, it effectively prevents issues related to excessive charging or discharging of the SM capacitors. Furthermore, as the fluctuations in the SM capacitor voltages diminish, the circulating current also decreases. These findings unequivocally demonstrate the efficacy of the proposed voltage-balancing algorithm for the MMC.

4.2. Experimental Results

To verify the proposed control strategy, a low-power experimental prototype of a three-phase MMC was developed, as demonstrated in Figure 7. The experimental parameters are listed in Table 1. The MMC is controlled using the "*μ-tech*" research and development control platform. The experimental results of the PQ, VSG, CVB-PQ, and CVB-VSG control strategies applied to the MMC are shown in Figures 8 and 9, with a change in the active power injected into the grid from 80 W to 120 W at time $t = 60$ s.
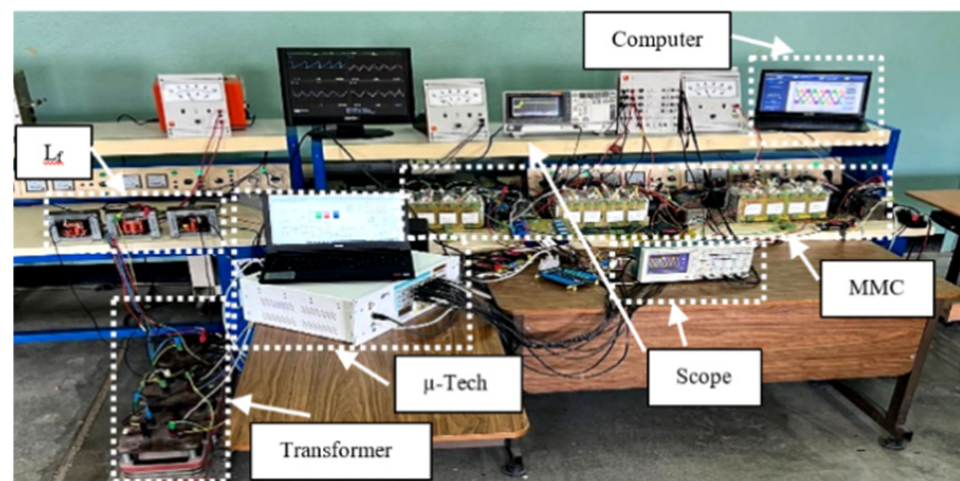

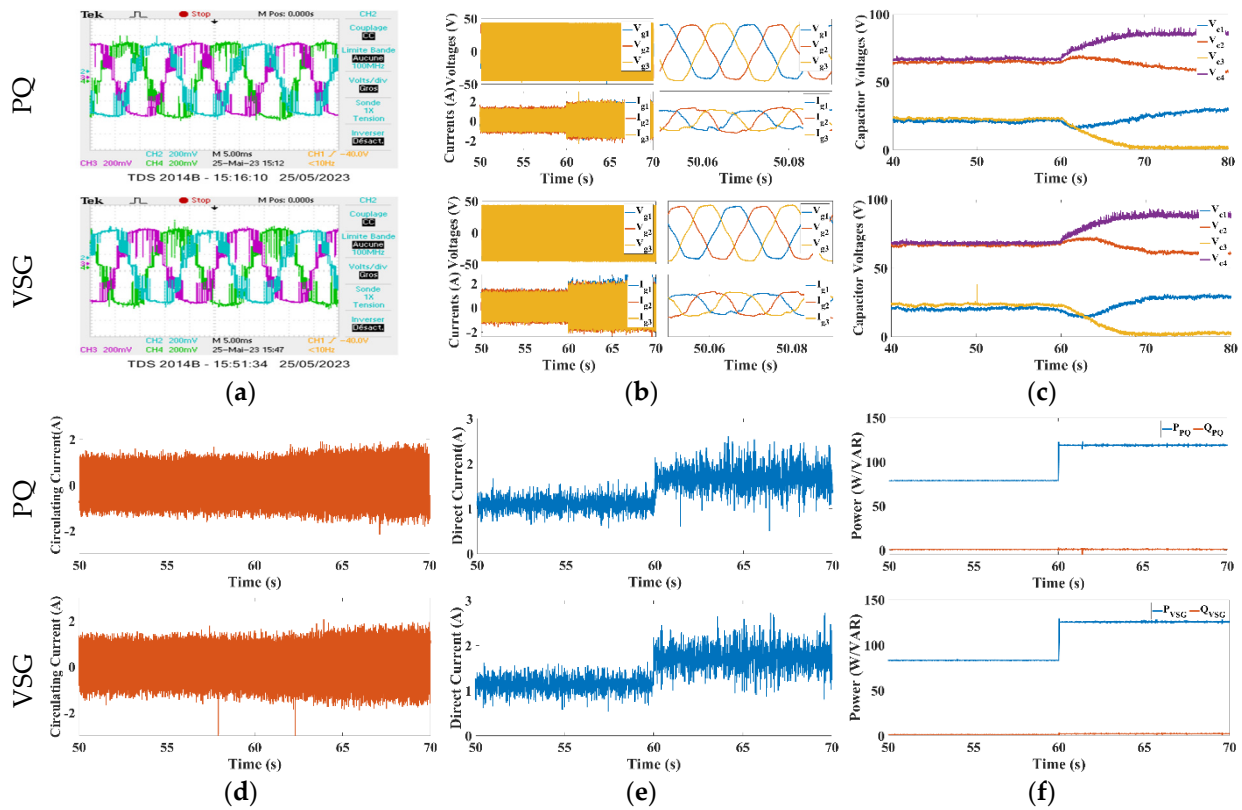**Figure 7.** Experimental platform of the three-phase MMC.

Figure 8. Experimental results of applying VSG and PQ control to the MMC. (**a**) Three-phase voltages of the MMC. (**b**) Three-phase voltages and currents of the grid. (**c**) Voltages of SM capacitors in phase B. (**d**) Phase A circulating current. (**e**) DC current. (**f**) Active and reactive power.
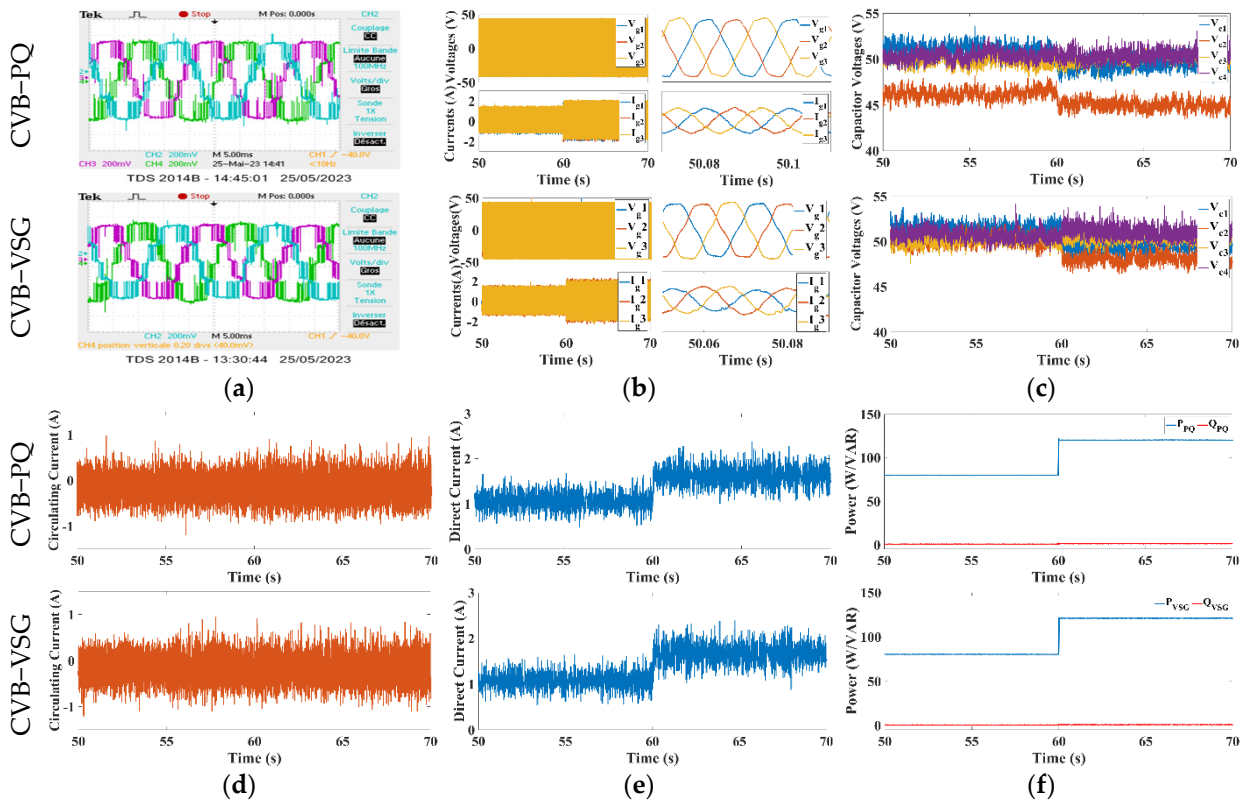

Figure 9. Experimental results of applying CVB−VSG and CVB−PQ control to the MMC. (**a**) Three-phase voltages of the MMC. (**b**) Three-phase voltages and currents of the grid. (**c**) Voltages of SM capacitors in phase B. (**d**) Phase A circulating current. (**e**) DC current. (**f**) Active and reactive power.

Figures 8a and 9a depict the steady-state waveforms of the MMC output voltage. It is evident that the waveform exhibits improved characteristics when utilizing the CVB-PQ and CVB-VSG control strategies (Figure 9a), where five balanced and stable levels are observed. In contrast, the PQ and VSG strategies (Figure 8a) result in unstable and unbalanced voltage levels, leading to the disappearance of internal levels.

Figures 8b and 9b illustrate the steady-state currents and voltages of the grid. The voltage waveform appears sinusoidal, while the current ranges from 1.5 A to 1.8 A, corresponding to variations in the power reference. Comparing the CVB-PQ and CVB-VSG control strategies (Figure 9b) with the PQ and VSG strategies (Figure 8b), it is evident that the former exhibit improved current waveforms with fewer fluctuations.

The voltages of the SM capacitors in phase B are presented in Figures 8c and 9c for the PQ and VSG control strategies, as well as the CVB-PQ and CVB-VSG control strategies, respectively. The voltages of the SM capacitors are paired and stable (1 and 3, 2 and 4), but they differ from the reference voltage Vdc/N, which is equal to 50 V. When there is a change in injected active power, the voltages of the SM capacitors become unbalanced and deviate towards either $V_{dc} = 100$ V or 0 V for the PQ and VSG control (see Figure 8c).

Without the implementation of the CVB method, the voltages across the SM capacitors are subject to substantial deviations, potentially compromising the stability and efficiency of the system. The capacitors within the SMs are engineered to handle defined active power thresholds, which are established based on the broader system architecture and the rated capacity of the MMC. Nevertheless, the observed voltage deviations stem not from inadequate capacitor sizing but from the suboptimal selection of which SMs are actively engaged or bypassed during operation. For the same capacitor, more capacitance would indeed reduce voltage deviations by lowering ripple ($\Delta V = I \Delta t/C$), but this comes at the cost of size, expense, slower dynamics, and potential inefficiency. The system may require more time to charge and discharge the capacitors during rapid power demand variations.

However, for the CVB-PQ and CVB-VSG control (see Figure 9c), the voltages of the SM capacitors remain stable, balanced, and equal to the reference voltage. The fluctuation range of the SM voltages is between 48 V and 51 V for the CVB-VSG control and between 44 V and 51 V for the CVB-PQ control.

The circulating currents of the PQ, VSG, CVB-PQ, and CVB-VSG controls are illustrated in Figures 8d and 9d, respectively. The circulating current is minimal, with lower fluctuations with the use of CVB-PQ and CVB-VSG controls (1.6 A and 1.4 A) compared to the PQ and VSG controls (3.6 A and 3.4 A), respectively.

Figures 8e and 9e depict the DC current for the PQ, VSG, CVB-PQ, and CVB-VSG controls, respectively. The DC current is more stable and exhibits lower fluctuations (1 A and 0.9 A) in the CVB-PQ and CVB-VSG controls compared to the PQ and VSG controls (fluctuations of 1.6 A and 1.4 A), respectively.

Figures 8f and 9f clearly show that the active and reactive powers follow the power references (ranging from 80 W to 120 W for active power and 0 VAR for reactive power) for the PQ, VSG, CVB-PQ, and CVB-VSG control strategies, respectively. A slight disturbance in active power (P = 120 W) is observed for the PQ and VSG control, whereas the CVB-PQ and CVB-VSG control exhibit greater stability.

We clarify that Figures 8a and 9a show the raw oscilloscope recordings of the voltages, captured directly using a Tektronix oscilloscope, thereby illustrating the real-time measured signals during the experimental tests. In contrast, Figures 8b–f and 9b–f present post-processed experimental data: the signals were captured using a data acquisition system and subsequently processed and evaluated within MATLAB. This analysis enabled the extraction and emphasis of critical parameters (including circulating current, DC voltage,

active power, reactive power, and others) while effectively removing unwanted noise to ensure the clarity and accuracy of the results.

The numerical data in Table 3, obtained from practical validations, serve as a robust foundation for the evaluation and comparison of the PQ, VSG, CVB-PQ, and CVB-VSG control methods. These practical validations offer real-world insights into the performance of each method, allowing for a comprehensive analysis of their effectiveness.

Table 3. Numerical data from practical validations for PQ, VSG, PQ-CVB, and VSG-CVB control.

Control	ΔIdc	ΔIcirc	ΔVc	Vcref–Vcestm
PQ	1.6 A	3.6 A	12 V	100 V
VSG	1.4 A	3.4 A	9 V	100 V
CVB-PQ	1 A	1.6 A	1.5 V	7 V
CVB-VSG	0.9 A	1.4 A	1.5 V	3 V

Based on the simulation and experimental results, SM capacitor voltage-balancing techniques like CVB provide an effective solution to enhance the stability and performance of MMC systems. The CVB-VSG control, in particular, offers several potential advantages, including simplicity, reliability, fast response, and the ability to adapt to dynamic variations. These advantages highlight the potential benefits of using CVB-VSG control for MMC systems.

5. Conclusions

A novel combined VSG control with a simplified CVB method has been presented for grid-connected MMC systems control. The proposed control structure integrates VSG for power sharing and inertia emulation, resulting in improved dynamic response, system stability, and a simplified CVB method for estimating and balancing the SM capacitor voltages.

Simulations and experimental tests were conducted to validate the effectiveness of the proposed control strategy, comparing it with the conventional PQ decoupled control approach. The results highlight the suitability of CVB-VSG for controlling MMC-based grid-connected systems. Additionally, the proposed control technique minimizes circulating current, reduces DC-side disturbances, eliminates the need for extensive sensor deployment, and reduces computational requirements.

Author Contributions: Conceptualization, H.B.; Methodology, H.B., F.K., A.B. and M.B.; Validation, F.K., A.B. and M.B.; Formal analysis, H.B., F.K., A.B., L.B. and M.B.; Investigation, H.B.; Data curation, H.B.; Writing—original draft, H.B.; Writing—review & editing, F.K., A.B., L.B. and M.B.; Visualization, F.K., A.B. and M.B.; Supervision, F.K. and M.B. All authors have read and agreed to the published version of the manuscript.

Institutional Review Board Statement: Not applicable.

Informed Consent Statement: Not applicable.

Data Availability Statement: No new data were created or analyzed in this study. Data sharing is not applicable to this article.

Conflicts of Interest: The authors declare no conflict of interest.

References

1. Cao, G.; Sun, K.; Jiang, S.; Lu, S.; Wang, Y. A modular DC/DC photovoltic generation system for HVDC grid connection. *Chin. J. Electr. Eng.* **2018**, *4*, 56–64.
2. Wang, S.; Zhou, L.; Wang, T.; Chen, T.; Wang, Y. Fast protection strategy for DC transmission lines of MMC-based MT-HVDC grid. *Chin. J. Electr. Eng.* **2021**, *7*, 83–92. [CrossRef]
3. Alemi-Rostami, M.; Rezazadeh, G. Selective harmonic elimination of a multilevel voltage source inverter using whale optimization algorithm. *Int. J. Eng.* **2021**, *34*, 1898–1904.
4. Chandio, R.; Chachar, F.; Soomro, J.; Ansari, J.; Munir, H.; Zawbaa, H.; Kamel, S. Control and protection of MMC-based HVDC systems: A review. *Energy Rep.* **2023**, *9*, 1571–1588. [CrossRef]
5. Hossain, M.; Shafiullah, M.; Abido, M. Battery Power Control Strategy for Intermittent Renewable Energy Integrated Modular Multilevel Converter-Based High-Voltage Direct Current Network. *Sustainability* **2023**, *15*, 2626. [CrossRef]
6. Shahnazian, F.; Adabi, J.; Pouresmaeil, E.; Catalão, J. Interfacing modular multilevel converters for grid integration of renewable energy sources. *Electr. Power Syst. Res.* **2018**, *160*, 439–449. [CrossRef]
7. Verdugo, C.; Candela, J.; Blaabjerg, F.; Rodriguez, P. Three-phase isolated multimodular converter in renewable energy distribution systems. *IEEE J. Emerg. Sel. Top. Power Electron.* **2019**, *8*, 854–865. [CrossRef]
8. Liu, X.; Li, G.; Zheng, T.; Yang, X.; Guerrero, J. Thyristor-pair-and damping-submodule-based protection against valve-side single-phase-to-ground faults in MMC-MTDC systems. *IEEE Trans. Power Deliv.* **2021**, *37*, 3257–3269. [CrossRef]
9. Vozikis, D.; Adam, G.P.; Rault, P.; Despouys, O.; Holliday, D. Enhanced modular multilevel converter for HVDC applications: Assessments of dynamic and transient responses to AC and DC faults. *IEEE J. Emerg. Sel. Top. Power Electron.* **2020**, *9*, 6997–7008. [CrossRef]
10. Reddy, G.A.; Shukla, A. The enhanced modular multilevel converter with dc fault blocking capability. *IEEE Trans. Power Electron.* **2023**, *38*, 8571–8582. [CrossRef]
11. Arévalo-Soler, J.; Sánchez-Sánchez, E.; Prieto-Araujo, E.; Gomis-Bellmunt, O. Impact analysis of energy-based control structures for grid-forming and grid-following MMC on power system dynamics based on eigen properties indices. *Int. J. Electr. Power Energy Syst.* **2022**, *143*, 108369. [CrossRef]
12. Soomro, J.; Akhtar, F.; Hussain, R.; Ansari, J.A.; Munir, H. A detailed review of MMC circuit topologies and modelling issues. *Int. Trans. Electr. Energy Syst.* **2022**, *2022*, 8734010. [CrossRef]
13. Barros, L.; Martins, A.; Pinto, J. A comprehensive review on modular multilevel converters, submodule topologies, and modulation techniques. *Energies* **2022**, *15*, 1078. [CrossRef]
14. Hasan, N.; Rosmin, N.; Osman, D.; Musta'amal, A. Reviews on multilevel converter and modulation techniques. *Renew. Sustain. Energy Rev.* **2017**, *80*, 163–174. [CrossRef]
15. Shen, K.; Zhao, D.; Zhao, G.; Wang, S. Photovoltaic supplied grid-connected modular multilevel converter with active power injection and reactive power compensation capability. In Proceedings of the IECON 2017-43rd Annual Conference of the IEEE Industrial Electronics Society, Beijing, China, 29 October–1 November 2017; pp. 7837–7842.
16. Nataj, S.H.; Gholamian, S.; Rezanejad, M.; Mehrasa, M. Virtual synchronous generator-based control of modular multilevel converter for integration into weak grid. *IET Renew. Power Gener.* **2023**, *17*, 3097–3107.
17. Belila, A.; Amirat, Y.; Benbouzid, M.; Berkouk, E.; Yao, G. Virtual synchronous generators for voltage synchronization of a hybrid PV-diesel power system. *Int. J. Electr. Power Energy Syst.* **2020**, *117*, 105677. [CrossRef]
18. Li, Z.; Li, H.; Zheng, X.; Gao, M. Virtual model predictive control for virtual synchronous generators to achieve coordinated voltage unbalance compensation in islanded micro grids. *Int. J. Electr. Power Energy Syst.* **2023**, *146*, 108756. [CrossRef]
19. Ali, H.; Li, B.; Xu, Z.; Liu, H.; Xu, D. Virtual synchronous generator design based modular multilevel converter for microgrid frequency regulation. In Proceedings of the 2019 22nd International Conference on Electrical Machines and Systems (ICEMS), Harbin, China, 11–14 August 2019; pp. 1–6.
20. Gobburi, H.; Borghate, V.; Meshram, P. Voltage Balancing method for Modular Multilevel Converter with Sensorless Operation. In Proceedings of the 2022 IEEE IAS Global Conference on Emerging Technologies (GlobConET), Arad, Romania, 20–22 May 2022; pp. 828–833.
21. Dekka, A.; Wu, B.; Zargari, N.; Fuentes, R. Dynamic voltage balancing algorithm for modular multilevel converter: A unique solution. *IEEE Trans. Power Electron.* **2015**, *31*, 952–963. [CrossRef]
22. Al-Khayyat, A.; Ridha, A.; Fadel, H. Performance analysis of capacitor voltage balancing in modular multilevel converter by sorting algorithm. *Int. J. Power Electron. Drive Syst.* **2022**, *13*, 1548. [CrossRef]
23. Zhu, Y.; Xiao, M.; Su, X.; Yang, G.; Lu, K.; Wu, Z. Modeling of conduction and switching losses for IGBT and FWD based on SVPWM in automobile electric drives. *Appl. Sci.* **2020**, *10*, 4539. [CrossRef]
24. Wang, C.; Xu, J.; Pan, X.; Gong, W.; Zhu, Z.; Xu, S. Impedance modeling and analysis of series-connected modular multilevel converter (MMC) and its comparative study with conventional MMC for HVDC applications. *IEEE Trans. Power Deliv.* **2021**, *37*, 3270–3281. [CrossRef]

25. Bensiali, H.; Khoucha, F.; Benrabah, A.; Belila, A.; Benbouzid, M. Comparative Analysis of Modular Multilevel Converters and Alternate Arm Converters for HVDC Applications. In *Artificial Intelligence and Heuristics for Smart Energy Efficiency in Smart Cities: Case Study: Tipasa, Algeria*; Springer: Cham, Switzerland, 2022; pp. 312–321.

26. Liu, X.; Sun, P.; Arraño-Vargas, F.; Konstantinou, G. Provision of synthetic inertia by alternate arm converters in VSC-HVDC systems. In Proceedings of the 2021 31st Australasian Universities Power Engineering Conference (AUPEC), Perth, Australia, 26–30 September 2021; pp. 1–5.

27. Bensiali, H.; Khoucha, F.; Benrabah, A.; Benbouzid, M. An Improved Model Predictive Control for the Virtual Synchronous Generator Based on Modular Multilevel Converters. *Electrotech. Rev. Elektroteh. Vestn.* **2024**, *91*, 193–202.

28. Ma, Y.; Lin, H.; Wang, Z.; Wang, T. Capacitor voltage balancing control of modular multilevel converters with energy storage system by using carrier phase-shifted modulation. In Proceedings of the 2017 IEEE Applied Power Electronics Conference and Exposition (APEC), Tampa, FL, USA, 26–30 March 2017; pp. 1821–1828.

29. Wang, S.; Liu, T.; Huang, X.; Yu, Y. Capacitor voltage balancing control with reducing the average switching frequency in MMC. *J. Eng.* **2019**, *2019*, 2375–2380. [CrossRef]

30. Veerendra, A.S.; Mohamed, M.R.; Peddakapu, K.; Sekhar, C.P. Minimization of total harmonic distortion and enhancing voltage level for hybrid multilevel converter with different sources. *Adv. Control Appl. Eng. Ind. Syst.* **2020**, *2*, e58. [CrossRef]

31. Muhammad, F.; Rasheed, H.; Ali, I.; Alroobaea, R.; Binmahfoudh, A. Design and control of modular multilevel converter for voltage sag mitigation. *Energies* **2022**, *15*, 1681. [CrossRef]

32. Babayomi, O.; Zhang, Z.; Dragicevic, T.; Hu, J.; Rodriguez, J. Smart grid evolution: Predictive control of distributed energy resources—A review. *Int. J. Electr. Power Energy Syst.* **2023**, *147*, 108812. [CrossRef]

33. Harbi, I.; Rodriguez, J.; Liegmann, E.; Makhamreh, H.; Heldwein, M.L.; Novak, M.; Rossi, M.; Abdelrahem, M.; Trabelsi, M.; Ahmed, M.; et al. Model-predictive control of multilevel inverters: Challenges, recent advances, and trends. *IEEE Trans. Power Electron.* **2023**, *38*, 10845–10868. [CrossRef]

34. Akbari, E.; Shadlu, M.S. Model Predictive Control of Alternate Arm Converter with a Short-Overlap Period Under Steady-State and Transient Conditions. In Proceedings of the 2023 14th Power Electronics, Drive Systems, and Technologies Conference (PEDSTC), Babol, Iran, 31 January–2 February 2023; pp. 1–7.

35. Elserougi, A.; Daoud, M.I.; Massoud, A.M.; Abdel-Khalik, A.S.; Ahmed, S. Investigation of sensorless capacitor voltage balancing technique for modular multilevel converters. In Proceedings of the IECON 2014-40th Annual Conference of the IEEE Industrial Electronics Society, Dallas, TX, USA, 29 October–1 November 2014; pp. 1569–1574.

36. Yin, T.; Wang, Y.; Wang, X.; Yin, S.; Sun, S.; Li, G. Modular multilevel converter with capacitor voltage self-balancing using reduced number of voltage sensors. In Proceedings of the 2018 International Power Electronics Conference (IPEC-Niigata 2018-ECCE Asia), Niigata, Japan, 20–24 May 2018; pp. 1455–1459.

37. Hashkavayi, M.B.; Barakati, S.M.; Haredasht, M.R.; Barahouei, V.; Torabi, S.H. Balancing of Capacitor Voltages with a Reduced Number of Voltage and Current Sensors in Alternate Arm Multilevel Converter (AAMC). In Proceedings of the 14th Power Electronics, Drive Systems, and Technologies Conference (PEDSTC), Babol, Iran, 31 January–2 February 2023; pp. 1–5.

38. Daoud, M.; Massoud, A.; Elserougi, A.; Abdel-Khalik, A.; Ahmed, S. Sensor-less operation of hybrid boost modular multilevel converter for subsea multiphase medium voltage drives. In Proceedings of the 2017 IEEE Southern Power Electronics Conference (SPEC), Puerto Varas, Chile, 4–7 December 2017; pp. 1–5.

39. Zoraghi-Jedi, M.; Barakati, S.M.; Rahmani-Haredasht, M.; Barahouei, V.; Yazdani, A. Capacitance health monitoring in the modular multilevel converter using a method with minimum number of sensors and computational burden. *Int. J. Circuit Theory Appl.* **2024**, *52*, 6343–6361. [CrossRef]

40. Abushafa, O.S.; Dahidah, M.S.; Gadoue, S.M.; Atkinson, D.J. Submodule voltage estimation scheme in modular multilevel converters with reduced voltage sensors based on Kalman filter approach. *IEEE Trans. Ind. Electron.* **2018**, *65*, 7025–7035. [CrossRef]

41. Wachal, R.; Jindal, A.; Dennetiere, S.; Saad, H.; Rui, Ø.; Cole, S.; Cole, S.; Zhang, L.; Song, Z.; Cole, S.; et al. *Guide for the Development of Models for HVDC Converters in a HVDC Grid*; Working Group B4.57, Cigre; CIGRE: Paris, France, 2014.